A Simple Approach for Making Viable Safe and High-Performances Lithium-Sulfur Battery

Lorenzo Carbone,[a] Thomas Coneglian,[b] Mallory Gobet,[c] Stephen Munoz,[c,d] Matthew Devany,[e] Steve Greenbaum,[c,*] and Jusef Hassoun[b,*]

[a] Chemistry Department, Sapienza University of Rome, Piazzale Aldo Moro, 5, 00185, Rome, Italy

[b] Department of Chemical and Pharmaceutical Sciences, University of Ferrara, Via Fossato di Mortara, 44121, Ferrara, Italy

[c] Department of Physics & Astronomy, Hunter College of the City University of New York, New York, New York 10065, United States

[d] Ph.D. Program in Physics, City University of New York, New York, NY 10016 United States

[e] Department of Chemistry and Biochemistry, Hunter College of the City University of New York, New York, New York 10065, United States

[*] Corresponding Authors: Jusef.hassoun@unife.it, sgreenba@hunter.cuny.edu

Keywords

Lithium/Sulfur, low-flammability, diethylene glycol dimethyl ether, carbon nanotubes, NMR/EIS

Abstract

We report an electrolyte with low-flammability, based on diethylene glycol dimethyl ether (DEGDME) dissolving lithium bis-trifluoromethane sulfonimidate (LiTFSI), and lithium nitrate ($LiNO_3$) for high performances lithium/sulfur battery. Self-diffusion coefficients, conductivity, and lithium transport number of the electrolyte are obtained by nuclear magnetic resonance and electrochemical impedance spectroscopy. Interface stability, lithium stripping/deposition ability, and electrochemical stability window of the electrolyte, are determined by voltammetry and impedance spectroscopy. The tests suggest conductivity higher than 10^{-2} S cm^{-1}, lithium transport number of about 0.5, electrochemical stability extending from 0V to 4.6V, and excellent compatibility with lithium metal. A composite cathode using sulfur and multi walled carbon

nanotubes (MWCNTs) is characterized in terms of structure and morphology by X-ray diffraction and scanning electron microscope. The study shows spherical flakes in which the carbon nanotubes protect the crystalline sulfur from excessive dissolution, and create the optimal host for allowing the proper cell operation. The Li/S cell reveals highly reversible process during charge/discharge cycles, fast kinetic, and lithium diffusion coefficient ranging from 10^{-12} to 10^{-10} cm^2 s^{-1}. The cell evidences a coulombic efficiency approaching 100%, capacity from 1300 mAh g^{-1} to 900 mAh g^{-1} and practical energy density higher than 400 Wh kg^{-1}.

Introduction

Among the several batteries proposed during the last decades, lithium ion battery is undoubtedly the most attractive one due to its remarkable energy and power contents [1,2]. Increasing interest on new electrochemical energy storage systems characterized by high performances has been recently triggered by the rapid spread of portable electronics, and the recent challenge of hybrid electric (HEVs), plug-in hybrid (PHEVs), and full electric (EVs) vehicles, suggested for limiting climate changes driven from excessive greenhouse gasses emission by massive use of fossil fuels [3–5]. Therefore, the emerging needs may be fulfilled by cheap, highly efficient and energetic batteries, rather than the most widespread lithium ion system in which the use of the expensive $LiCoO_2$ limits the energy density to about 550 Wh Kg^{-1} with respect to the cathode mass and drastically increases the costs [6]. Lithium/sulfur battery, due to limited cost, very high theoretical capacity (1675 mAh g^{-1}) and energy density (3600 Wh Kg^{-1}), as well as environmental compatibility, appears one of the most suitable candidate for overcoming the intrinsic limits of the common batteries [7]. The Li/S electrochemical reaction, i.e., $16Li + S_8 \leftrightarrow 8Li_2S$ [8,9], evolves between 2.4V and 2.1V and leads to phase changes [10] with production of several polysulfides moieties and radicals [11–13]. Unfortunately, polysulfides dissolve into the electrolytes during the discharge, shuttle between cathode and anode during charge, and directly react by electrochemical short circuit with lithium leading to low coulombic efficiency, loss of

cathode mass, and fast capacity decay [14]. Organic carbonate solutions commonly used in the commercial lithium ion battery particularly suffer from this issue as well as instability against Li metal, hence a new classes of electrolyte, mainly based on ether bond, such as dioxolane (DOL), dimethoxyethane (DME), end-capped glymes, and polyethyleneoxide (PEO), appeared valid alternative for application in Li/S battery [15–17]. DOL/DME mixture containing LiTFSI salt is presently the most used electrolyte for Li/S battery, due to the high ion conductivity promoted by the ether bond which actually drives the lithium ion transport [18]. This electrolyte is generally upgraded by the use of $LiNO_3$ as sacrificial film forming agent to stabilize the lithium/electrolyte interface [19–21], while further improvements of the cell performances may be obtained by the employment of alternative separators added to carbon to physically trap the polysulfides on the cathode side [22–24], or by metal oxides to chemically retain the polysulfides on electroactive sites of the cathode surface [25–27]. Many efforts have been devoted to develop composite cathodes combining sulfur and functional carbons, such as nano-sphere [28], carbon nanosheets[29], nanotubes [30], and mesoporous carbons [31], suitable for efficiently hosting sulfur and strongly adsorbing polysulfides during cycles. However, the most successful approaches involved very volatile and flammable DOL-DME-based electrolyte [32], or very safe but poorly conductive viscous glyme-based ones [33–35], as well as highly engineered and not particularly cost effective sulfur cathodes [36], which have led to poorly scalable Li/S cell. A comparative study focused on the determination of the most suitable thermal, transport and electrochemical characteristics of various ether-based electrolytes differing by chain length, using the lithium triflate ($LiCF_3SO_3$) salt, suggested the DEGDME glyme-based electrolyte as promising material for application in lithium cell [17]. The study reported a proof of concept Li/S battery using a ball milled S-C composite which was preliminarily studied during 25 cycles at low current rate (C/20 = 83.75 mA g^{-1}). Therefore, we study in this work a new electrolyte based on DEGDME solvent, LiTFSI salt, and $LiNO_3$ additive, advantageously combining the high safety level of the glyme, and a high conductivity expected by the low viscosity and the high solvating ability of the short-chain

DEGDME. The solution is investigated by a relevant detail, suitably combining NMR and electrochemistry at various temperatures, and adopted as the electrolyte media in a high performances Li/S cell in combination with a S-MWCNTs composite prepared by melting commercial sulfur and MWCNTs, and cast on a carbon cloth with increasing loadings. The sulfur electrode is fully studied, and the kinetic aspects of its electrochemical process in lithium cell are originally clarified by adopting the Randles-Sevcik equation during cycling voltammetry. The improved characteristics of the electrode/electrolyte configuration here reported lead to substantial increase of the cell cycle life (to over 120 cycles), the rate capability and the energy density. The high safety content and significant performances of the Li/S battery configuration studied in this work may actually promote a sustainable scaling-up of an efficient high energy storage system.

Experimental

Materials. Diethylene glycol dimethyl ether $(CH_3OCH_2CH_2)_2O$ (Sigma-Aldrich), denoted hereafter by DEGDME, was dried before use with molecular sieves (5 Å) until the water content was below 10 ppm as measured by 831 Karl Fischer Coulometer (Metrohm). Lithium bis-trifluoromethanesulfonimidate ($CF_3SO_2NLiSO_2CF_3$, LiTFSI) and lithium nitrate ($LiNO_3$), from Sigma-Aldrich, were separately dried under vacuum overnight at 80 °C. All the samples were subsequently handled in argon filled glove box, with oxygen and moisture content lower than 1 ppm. LiTFSI was dissolved in DEGDME by a salt to solvent ratio of 1 mol kg^{-1} to obtain the electrolyte (indicated by DEGDME-LiTFSI). The electrolyte for battery application (DEGDME-LiTFSI-$LiNO_3$) was prepared by dissolving $LiNO_3$ (film forming sacrificial additive with salt to solvent ratio of 1 mol kg^{-1}) and LiTFSI (ions conductor with salt to solvent ratio 1 mol kg^{-1}) in DEGDME. The S-carbon powder was prepared by melting elemental sulfur (Sigma-Aldrich) at 135°C and mixing with multi-walled carbon nanotubes MWCNTs (from Sigma-Aldrich) by a 60:40 S to C weight ratio. The sample was stirred 3 hours under heating at 135°C in order to obtain a homogeneous mixture, cooled down to room temperature and refined by mortar. The electrode

slurry was prepared by mixing the S-MWCNTs-S powder, Super P Carbon conductive additive (Timcal) and polyvinylidene difluoride binder (PVdF; Solvay Solef) binder in 80:10:10 weight ratio, using N-methylpyrrolidone (NMP) as solvent. The slurry was cast onto carbon cloth support (GDL ELAT) by the Doctor Blade method with a wet thickness varying from 300 µm to 600 µm, in order to obtain various sulfur loadings. The electrode foils were punched into 10 mm and 16 mm disks, dried for 48 hours at 60°C under vacuum before assembling the cell in the argon filled glovebox with oxygen and water content lower than 1 ppm. The sulfur loading of the final electrodes was 2, 2.5, 3 and 4 mg cm^{-2}.

Electrolyte Characterization. The self-diffusion coefficient of the ^{1}H, ^{19}F, and ^{7}Li nuclei in the DEGDME-LiTFSI electrolyte were measured by a Bruker 400 Advance III NMR spectrometer within screw-cap gastight NMR tubes in order to overcome possible evaporation along the temperature scan from 20°C to 70°C. The data were collected every 10 °C for each nucleus using a double-stimulated echo sequence with pulse field gradients (PFG) to suppress convection. The gradient pulse strength was increased linearly in 32 steps from 1 to 45 G cm^{-1}, the gradient pulse duration (δ) was of 1.4 − 4 ms with a diffusion delay (Δ) of 200 − 400 ms. Eddy current effects were avoided by using a longitudinal eddy-current delay (LED) of 5 ms.

The self-diffusion coefficients were calculated by eq. 1:

$$I = I_0 \, e^{-D\gamma^2 g^2 \delta^2 \left(\Delta - \frac{\delta}{3}\right)} \qquad (1)$$

where I is the signal integral, D is the self-diffusion coefficient, γ is the gyromagnetic ratio of the studied nucleus, g is the gradient pulse strength, δ is the gradient pulse duration and Δ is the diffusion delay. The error on the self-diffusion coefficient is about 3-5% [37].

The lithium transport (t^{+}) number was calculated from the self-diffusion coefficient by eq. 2:

$$t^{+} = \frac{D_{Li}}{D_{Li} + D_{LiTFSI}} \qquad (2)$$

where D_{Li} is the self-diffusion coefficient of lithium, and D_{LiTFSI} is the self-diffusion coefficient of the TFSI anion [$N(SO_2CF_3)_2^-$].

Ion conductivity was calculated from the self-diffusion coefficients by the Nernst-Einstein equation (eq. 3):

$$\delta_{NMR} = \frac{F^2[C]}{RT}\ (D_{Li} + D_{CF_3SO_3}) \qquad (3)$$

where δ_{NMR} is the conductivity determined by the NMR, F is the Faraday constant (96485 C), [C] is the concentration of the salt in the electrolyte (mol cm^{-3}), R is the ideal-gas constant (8.314472 J K^{-1} mol^{-1}), T is the temperature (K), D_{Li} and D_{LiTFSI} are the corresponding self-diffusion coefficients.

Ion conductivity was also measured by electrochemical impedance spectroscopy (EIS) using a VersaSTAT MC Princeton Applied Research-AMETEK potentiostat. A symmetrical stainless steel/ stainless steel 2032 coin-cell with a Teflon ring separator was used to ensure a fixed cell constant during the measurements. The data were collected every 10°C by heating and cooling the cell within 40°C - 80°C temperature range using a signal amplitude of 10 mV and in a 0.1 Hz-0.5 MHz frequency range. The conductivity values determined by NMR (δ_{NMR}) and measured by EIS (δ_{EIS}) were used to obtain the ion association degree (α) of the LiTFSI salt by the eq. 4:

$$\alpha = (1 - \frac{\delta_{EIS}}{\delta_{NMR}}) \qquad (4)$$

Lithium/stripping deposition test was carried out in a symmetrical lithium/lithium 2032-coin cell using a current of 0.1 mA cm^{-2} with a step time of 1 hour at 23 °C, the test was performed by a MACCOR 4000 series Battery Test System. The electrochemical anodic stability widow was evaluated by linear sweep voltammetry (LSV) using a VersaSTAT MC Princeton Applied Research-AMETEK potentiostat, with scan rate of 0.1 mV s^{-1} within OCV and 5V vs Li/Li^+ with a three electrode Swagelok T-cell equipped with lithium metal reference and counter electrodes, and a Super P carbon coated on carbon cloth working electrode. The same cell configuration and

instrument were used to study the cathodic electrochemical stability of the electrolytes by cyclic voltammetry (CV). The CV was performed with a scan rate of 0.1 mV s^{-1} in a 0 - 2 V vs Li/Li^+ potential range. The lithium/electrolyte interface chemical stability was evaluated by electrochemical impedance spectroscopy in a symmetrical lithium/lithium 2032-coin cell, acquiring with a VersaSTAT MC Princeton Applied Research-AMETEK the impedance spectra every day, using 10 mV signal amplitude in a 0.1 Hz - 0.5 MHz frequency range. The impedance spectra were analyzed by non-linear least squares fit (NLLSQ) using a Boukamp software [38,39]. Only fitting results with a chi-square (χ^2) lower than 10^{-4} were accepted. Flammability tests was performed on the DEGDME-LiTFSI-$LiNO_3$ electrolyte by direct ignition of the solution in standard room environment.

S-MWCNTs electrode characterization. A Bruker instrument x-ray diffractometer equipped with a Cu Kα source and a graphite monochromator in the 2θ/θ scanning mode was used to evaluate the structure of the sulfur-carbon electrode. The morphology of the sample was studied by a scanning electron microscopy (SEM, Zeiss EVO 40) with a thermionic electron gun equipped with LaB_6 crystal and by energy dispersive x-ray spectrometry (SEM-EDX) by a X-ACT Cambridge Instruments analyzer.

The Li/DEGDME-LiTFSI-$LiNO_3$/S-MWCNTs cell. Cyclic voltammetry of S-MWCNTs working electrode with a sulfur loading of 3 mg cm^{-2} was performed in a three-electrode cell with lithium metal as reference and counter electrode using the DEGDME-LiTFSI-$LiNO_3$ as the electrolyte. The test was performed with a scan rate of 0.1mV s^{-1} in a 1.8 V - 2.8 V potential range. A second cyclic voltammetry test in the above reported potential range was carried using the same cell configuration at various scan rates (i.e., 0.1, 0.2, 0.3, 0.4 and 0.5 mV s^{-1}) in order to evaluate the Li^+ diffusion coefficients (D) within the cathode material by the Randles-Sevcik equation (Eq. 5) [40,41]:

$$I_p = o.4463\ z\ FAC\ \sqrt{\frac{zF\nu D}{RT}} \qquad (5)$$

where I_p is the peak current value (A), z is the number of exchanged electrons for the taken peak, F is the Faraday constant (96485 C mol^{-1}), A is the electrode geometric area (cm^2), C is the Li^+ concentration in the active material (mol cm^{-3}), ν is the scan rate (V s^{-1}), R is the gas constant (J K^{-1} mol^{-1}), and T is the used temperature (K). The CV tests were performed at 23°C by a VersaSTAT MC Princeton Applied Research-AMETEK potentiostat.

Galvanostatic cycling tests of the electrodes with various sulfur loadings (2 mg, 2.5, 3 and 4 mg cm^{-2}) were carried out at the current rate of C/3, while the electrode with a sulfur mass loading of 4 mg cm^{-2} required a current of C/8 for significant cycling (1C = 1675 $mAhg^{-1}$), in a 1.9V – 2.8V voltage range. A cycling test at various c-rates (i.e., C/10, C/8, C/5, C/3, C/2 and 1C) was performed using an electrode with 3 mg cm^{-2} sulfur loading in a 1.9 V – 2.8 V voltage range. Cycling tests prolonged over 100 cycles were performed at C/3 in a 1.9 V – 2.8 V voltage range and at 1C in a 1.8 V – 2.8 V voltage range, using an electrode with 3 mg cm^{-2} sulfur loading. All the galvanostatic tests were performed by a MACCOR 4000 series Battery Test System using a 3032-coin cells (electrode geometric surface 1.54 cm^2) filled by 50 µl of the DEGDME-LiTFSI-$LiNO_3$ electrolyte at 23°C. Cells were cycled following 3 hours of rest at the OCV.

Results and discussion

Ions and solvent molecules mobility represents a key factor in determining the electrolyte characteristics for application in the energy storage devices. A very suitable protocol for determining such an important parameter has been developed in our previous studies[42–44] by combining NMR and EIS measurements in a blocking electrode cell, and adopted in this work for the study of the new LiTFSI-DEGDME electrolyte (Figure 1). It is worth mentioning that $LiNO_3$ is not considered by this protocol since it is added as a sacrificial film forming agent for passivating the lithium metal which is consumed by the initial cycling stages and, therefore, excluded from ion conduction mechanism [45,46]. Figure 1A shows the self-diffusion coefficient of the ^1H, ^{19}F, and ^7Li nuclei in the electrolyte, determined between 20°C and 70 °C. All the coefficients increase with

increasing temperature, however the glyme chain shows higher mobility (D_H) in the whole range with respect to the ions nuclei as indeed observed other ether based electrolytes [47], while lithium and anion (D_{Li} and D_F, respectively) show similar mobility. The lithium transport number, calculated by eq. 2 (experimental section) and reported in Figure 1B reveals a value ranging from 0.47 at 20°C to 0.49 at 70 °C, which is expected to ensure a fast charge transfer at the electrode/electrolyte interface in lithium battery. It is important to point out that the apparent transport number value close to 0.5 is at least partly a consequence of ion association, which results in correlated motion with similar cation and anion diffusion coefficients. However as will be discussed next, these electrolytes exhibit markedly less ion association than glymes with other salts [48]. Nonetheless, NMR-determined Li^+ transport numbers in electrolytes as disparate as high molecular weight PEO and liquid carbonates are more typically around 0.2 – 0.3. Notably, the ionic conductivity in the current system shows a practical value as high as 10^{-2} S cm^{-1} as measured by EIS (δ_{EIS} in Figure 1C) which is very suitable for high rate applications. The conductivity observed for the DEGDME-LiTFSI electrolyte is much higher than that observed for other glyme solutions reported previously [43], and comparable to DOL/DME-based electrolyte, which is the one commonly used in lithium-sulfur battery [48]. The apparent conductivity of the electrolyte calculated by eq. 3 using the NMR self-diffusion coefficients of the ions (δ_{NMR} in Figure 1C), may be combined in eq. 4 with the practical value of the conductivity determined by EIS (δ_{EIS} in Figure 1C) for the evaluation of the ion association degree (α) which is reported in Figure 1D (see experimental section for equations). The figure reveals relatively low ion association for the DEGDME-LiTFSI electrolyte with respect to solutions based on $LiCF_3SO_3$ salt which confirms the higher dissociation ability of LiTFSI with respect to $LiCF_3SO_3$ [43,44,47,49]. This important characteristic is ascribed to the interaction between salt and solvent which is temperature-dependent: an increasing interaction between solvent molecules and salt ions hinders the ion association and promotes the free ions in the solution. Indeed, DEGDME-LiTFSI electrolyte shows the decrease of α from 0.7 at 40°C to 0.45 at 70°C in Figure 1D. This presents a very interesting

contrast with previous studies involving $LiCF_3SO_3$ [43,44,47] as the electrolyte salt, in which it was found that ion association actually increases with increasing temperature due the decreasing solvating ability of the elevated temperature solvent with a salt that is more prone to ion pairing.

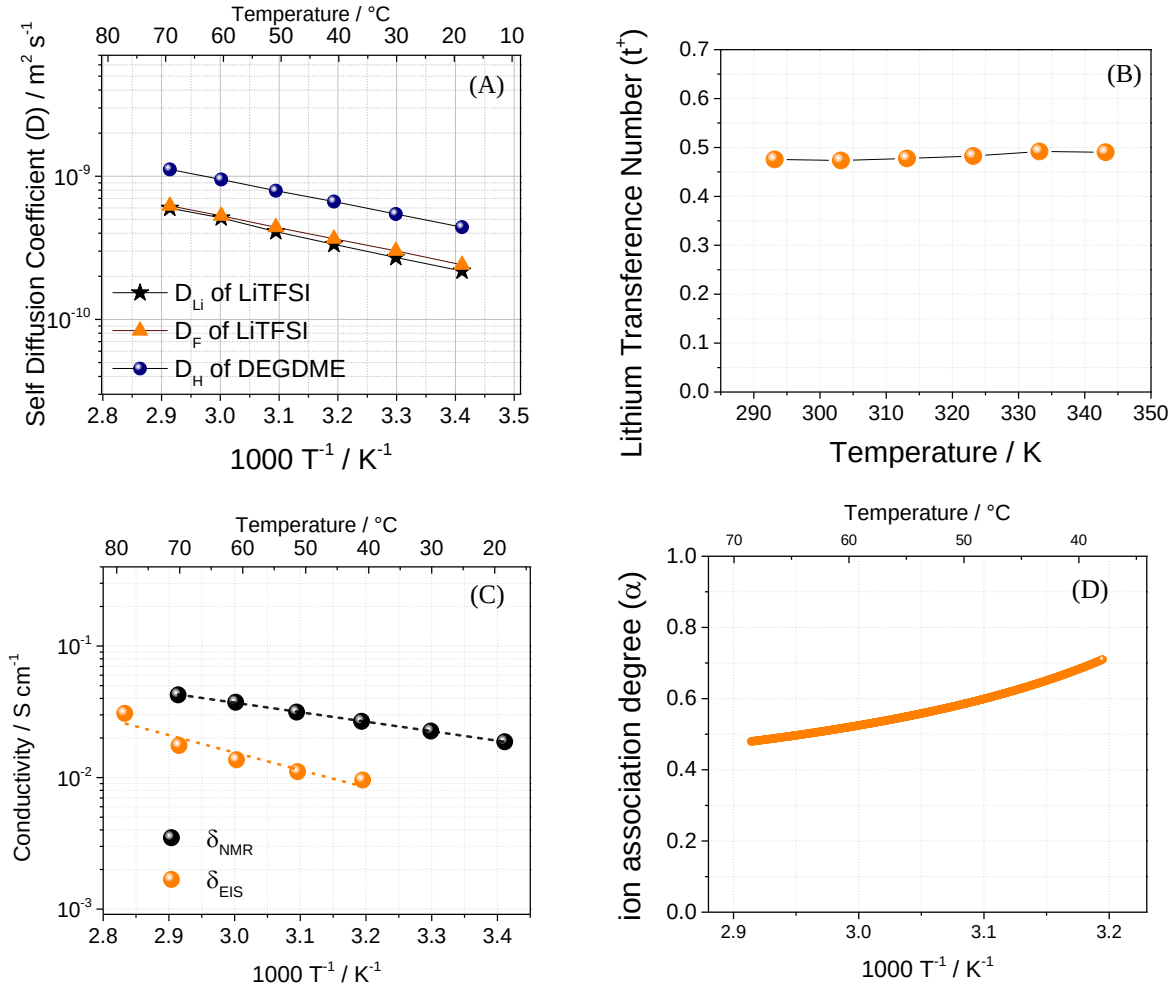

Figure 1. (A) Self-diffusion coefficient of ^{7}Li, ^{19}F and ^{1}H in the DEGDME-LiTFSI electrolyte (1mol kg^{-1}) determined by PFG NMR. (B) Conductivity Arrhenius plots of the DEGDME-LiTFSI electrolyte performed using electrochemical impedance spectroscopy (EIS) by heating and cooling the sample in the temperature range between 40°C and 80 °C in a coin-cell, with signal amplitude of 10 mV within 500 MHz− 100 Hz frequency range. (C) lithium transport number (t^+) calculated from the self-diffusion coefficient values using equation (2), and (D) ion association degree (α) determined by equation (3) using the conductivity values determined by EIS (δ_{EIS}) and the values obtained from the self-diffusion coefficient (δ_{NMR}) by Nernst Einstein equation (4). See experimental section for equations.

The addition of $LiNO_3$ to the electrolyte has a crucial role in allowing its use in Li/S cell since this sacrificial salt chemically reacts and passivates the lithium metal, thus avoiding further side reactions both with the electrolyte components and with possible dissolved polysulfides [50]. Therefore, we have studied the chemical stability of the interface between DEGDME-LiTFSI-$LiNO_3$ solution and lithium, as well as the electrochemical stability windows of the electrolyte (Figure 2). The galvanostatic lithium stripping/deposition in symmetrical cell reported in Figure 2A reveals an average overvoltage of 0.02 V after 12 days, slightly changing during the initial stages of the test and finally stabilizing due to chemical formation, partial dissolution and consolidation of a solid electrolyte interphase (SEI) film [51]. A similar trend is observed over time for the interface chemical stability detected by impedance spectroscopy in Figure 2B (corresponding Nyquist plots in inset). The test evidences an initial fluctuation of the resistance from 250 to 700 Ω, and a final drift to 500 Ω as the SEI is formed and stabilized [52]. The DEGDME-LiTFSI-$LiNO_3$ electrolyte is further studied by voltammetry, both in the cathodic region (CV in Figure 2C) and in the anodic one (LSV in Figure 2D). The first CV cycle in Figure 2C exhibits irreversible peaks at 1.5 V and 0.8 V vs Li^+/Li, due to reduction of the electrolyte and electrochemical formation of the SEI, while the subsequent cycles reveal the reversible lithium insertion/de-insertion into amorphous Super-P carbon at about 1V and 0.1 V vs Li^+/Li, as well as possible lithium deposition/stripping at very low potentials (i.e., at about 0 V vs Li^+/Li) [53], without any further side reaction. The LSV of Figure 2D indicates for the electrolyte an anodic stability extended above 4.6V vs Li^+/Li, which is a suitable range for application in several lithium battery configurations, including the Li/S one which operates at about 2.1-2.4 V [54].

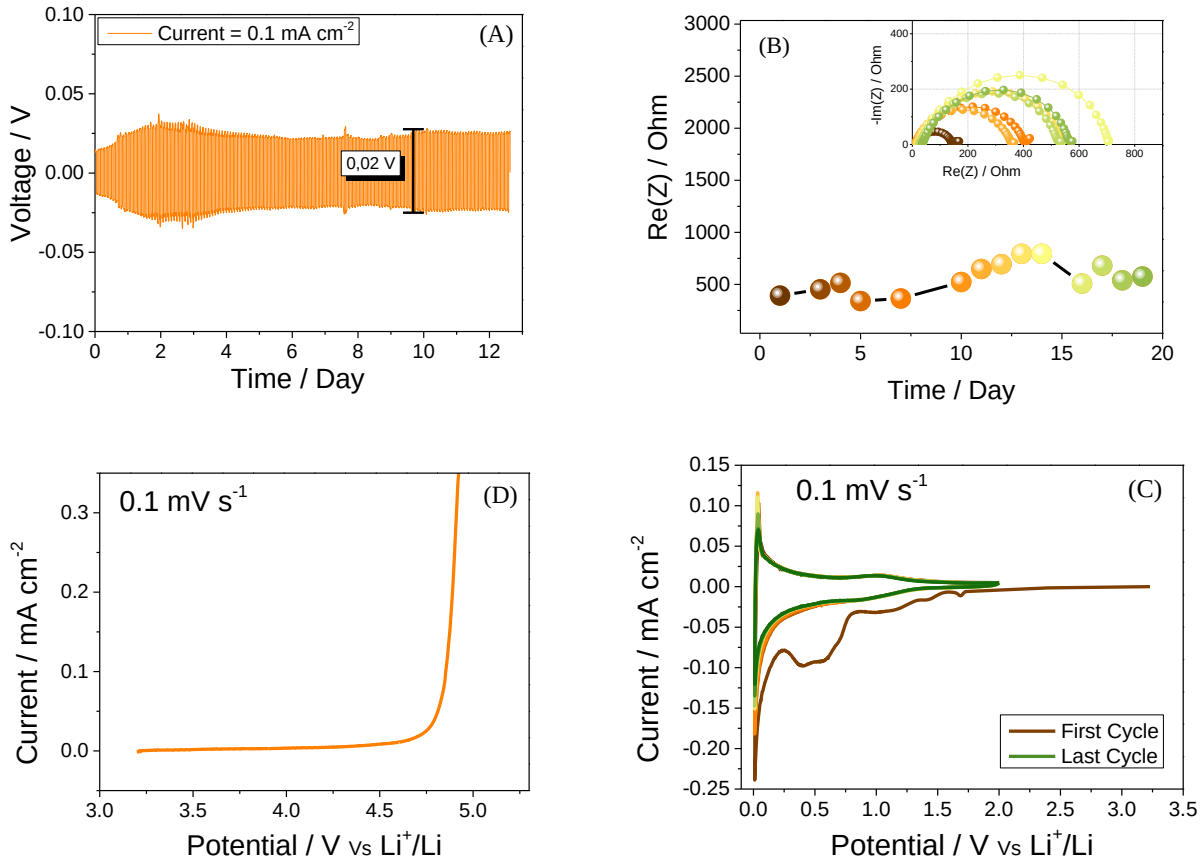

Figure 2. (A) Voltage versus time profile of lithium deposition/stripping galvanostatic test performed by applying a 0.1 mA cm^{-1} current to symmetrical Li/DEGDME-LiTFSI/Li cell. (B) Time evolution at 23°C of the lithium/electrolyte interface resistance performed in symmetrical Li/DEGDME-LiTFSI/Li cell using electrochemical impedance spectroscopy with signal amplitude of 10 mV within 500 MHz−100 mHz frequency range. (C) Cyclic voltammetry (CV) using potential limits of 0.01 V - 2 V and (D) linear sweep voltammetry (LSV) of the DEGDME-LiTFSI electrolyte in a tree electrode cell using a carbon coated on Cu and Al substrate, respectively, as the working electrode and lithium metal as counter and reference electrode. Scan rate 0.1 mV s^{-1}. Temperature 23°C.

Beside high conductivity, chemical and electrochemical stability, another suitable characteristic of the electrolyte, particularly attractive for a safe application in high energy lithium metal cells, is represented by its low flammability observed in Figure 3 which evidences missing evolution of fire by a direct ignition (see also Experimental section). Despite the material safety

data sheet (MSDS) of DEGDME solvent indicates possible flammability, we suppose that the high flash point and the low vapor pressure of this glyme make it lowly flammable when exposed to direct flame, such as in the test performed in our laboratory. A direct test in battery is certainly required to fully proof the characteristics of the DEGDME based electrolyte, however the preliminarily test herein reported suggests its higher safety with respect to the conventional carbonate based solutions.

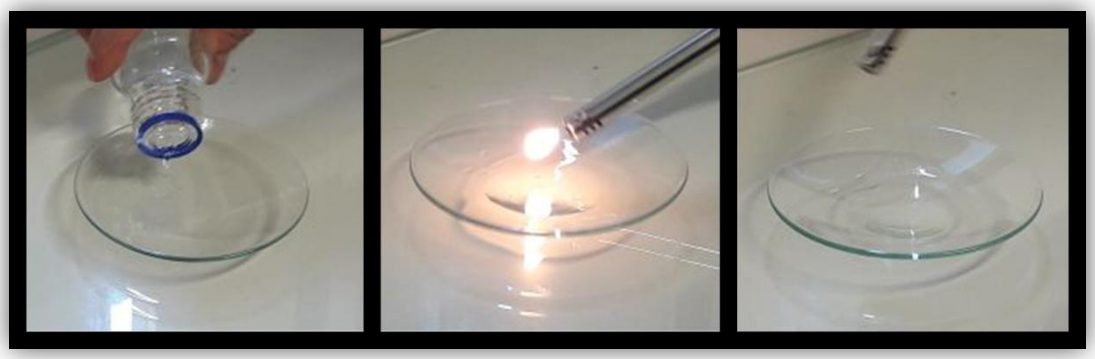

Figure 3. Flammability tests performed by direct ignition of a DEGDME LiTFSI $LiNO_3$ electrolyte sample in standard room environment.

The DEGDME-LiTFSI-$LiNO_3$ electrolyte is subsequently studied in a Li/S cell using a cathode prepared by melting S and mixing with MWCNTs (see experimental section), i.e., a simple technique leading to a crystalline material (XRD in Figure 4A) in which the orthorhombic sulfur S_8 (PDF # 85-0799) and the hexagonal MWCNTs are intimately mixed. Pristine tubes of carbon (SEM in Figure 4B) with micrometeric length (4 µm) and nanometric diameter (10-30 nm) surround the sulfur to form a spherical-shape composite with a size of about 10-25 µm (SEM in Figure 4C). Indeed, the EDX mapping in Figure 4D indicates that the S-MWCNTs sample is characterized by the presence of sulfur mainly in the core and MWCNTs in the shell with homogeneous distribution. This spherical-like, core-shell morphology enables a very important characteristic which may allow efficient ion and electron conduction into the electrode, hence satisfactory rate capability, in particular considering the insulating character of sulfur [55]. Furthermore, a homogeneous

distribution of MWCNTs at the particles shell may partially prevent the active material loss caused by soluble polysulfides formation during the electrochemical process [56]. It is worth mentioning that the use of a porous carbon cloth (Figure S1 in Supplementary Information) instead of aluminum as the electrode support represents a viable strategy to efficiently host possible dissolved species at the cathode/electrolyte interface, avoid their migration through the cell, thus improving the cell cycling stability. Another relevant characteristic of the material is represented by a straightforward synthetic pathway which allows easy and low cost preparation, thus leading to the reduction of the cost of the battery [57].

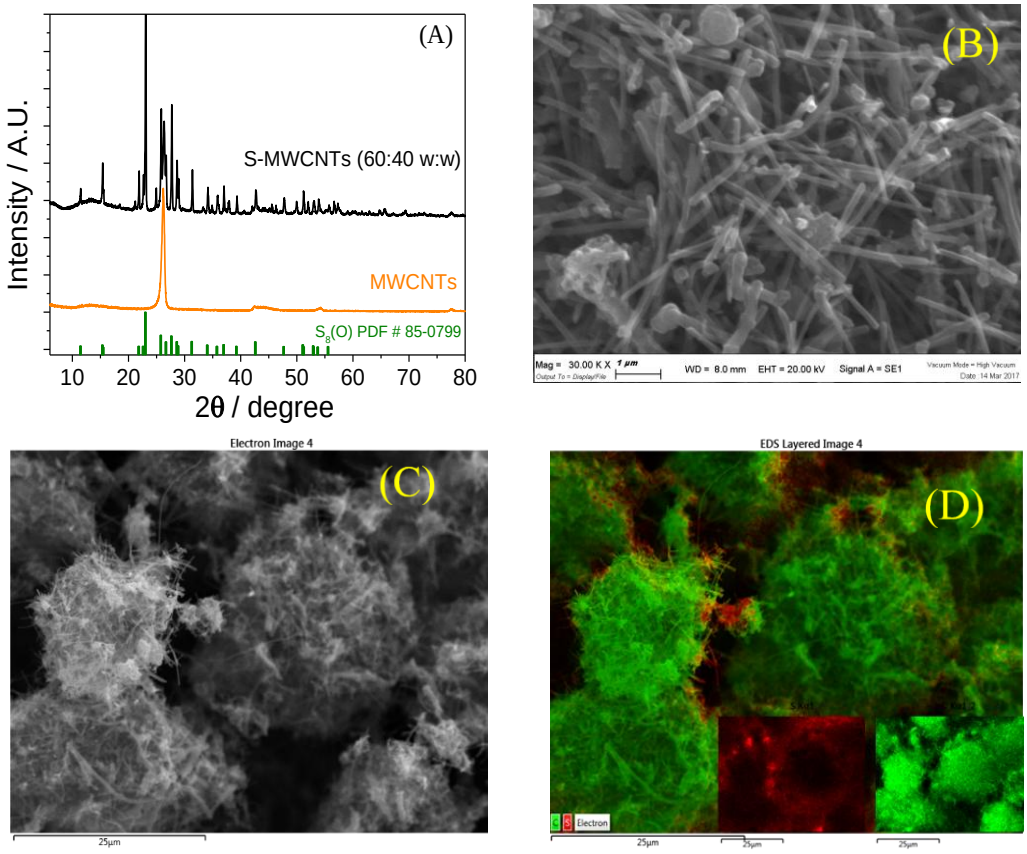

Figure 4. (A) X-ray diffraction patterns (XRD) of the S-MWCNTs composite. (B) Scanning electron microscopy (SEM) image of the pristine MWCNTs powder. (C) SEM image and (D) corresponding energy dispersive x-ray spectroscopy (EDX) mapping the S-MWCNTs composite. Carbon and sulfur are depicted by green and red color, respectively, in the EDX map.

The CV profiles of the Li/DEGDME-LiTFSI $LiNO_3$/S-MWCNTs cell at a constant scan rate (0.1 mV s^{-1}) reported in Figure 5A exhibit during the first cycle (black line) the characteristic shape ascribed to the electrochemical process of lithium and sulfur [54], with formation of long chain polysulfides (i.e., Li_2S_8, Li_2S_6) at 2.3 V vs. Li^+/Li and of short-chain species (i.e., Li_2S_4, Li_2S_2 Li_2S) at 1.9 V vs. Li^+/Li in the cathodic scan,[58] which are oxidized back by a merged double peak centered at about 2.4 vs. Li^+/Li due to the multi-electron charge reaction during anodic scan [12]. The subsequent cycle (dark green line) reveals an increase of the reduction potentials to 2.4 and 2 V vs. Li^+/Li, i.e., a decrease of the cell polarization, as well as an increase of the peaks intensity which may be likely ascribed to the decrease of the electrode resistance by the diffusion of the lithium ions into the material and the formation of lithiated species [59]. This trend is well justified by Figure 5B which displays the Nyquist plots of the impedance spectroscopy tests performed before and after the CV cycles. Indeed, the figure shows a remarkable decrease of the cell impedance from about 250 Ω at the OCV to about 10 Ω after the CV cycles. This process suggests the use of activation cycles and proper voltage cutoff tuning for suitable cycling of the cell, even at higher C-rates as will be shown hereafter. However, the CV cycles of Figure 5A evidence a slight reduction of the peak intensity by cycling after the second cycle, thus suggesting partial dissolution of the electrode by formation of polysulfides. The lithium diffusion into the electrode is further investigated by CV by increasing the scan rate (Figure 5C), using the Randless-Sevcik equation (eq. 5) according to which the peak current (I_p) is proportional to the square root of the scan rate, with a slope that depends on the lithium diffusion coefficient (D_{CV})[40]. Considering the overall process of the lithium with sulfur, summarized by using $2Li + S \leftrightarrows Li_2S$, in order to simplify the determination of D_{CV} we have attributed one electron to each reduction peak, and two electrons to the oxidation merged peak, despite the complex multiple step reaction mechanism [58]. This assumption allows the determination of the Li^+-diffusion coefficient at the various states of charge (Figure 5D), i.e., at about 2.5 V vs Li^+/Li during charge (corresponding linear fit in Figure S2A of Supplementary Information), 2.4 V vs Li^+/Li during discharge (linear fit in Figure S2B of Supplementary

Information) and 1.9 V vs Li^+/Li during discharge (linear fit in Figure S2C of Supplementary Information).

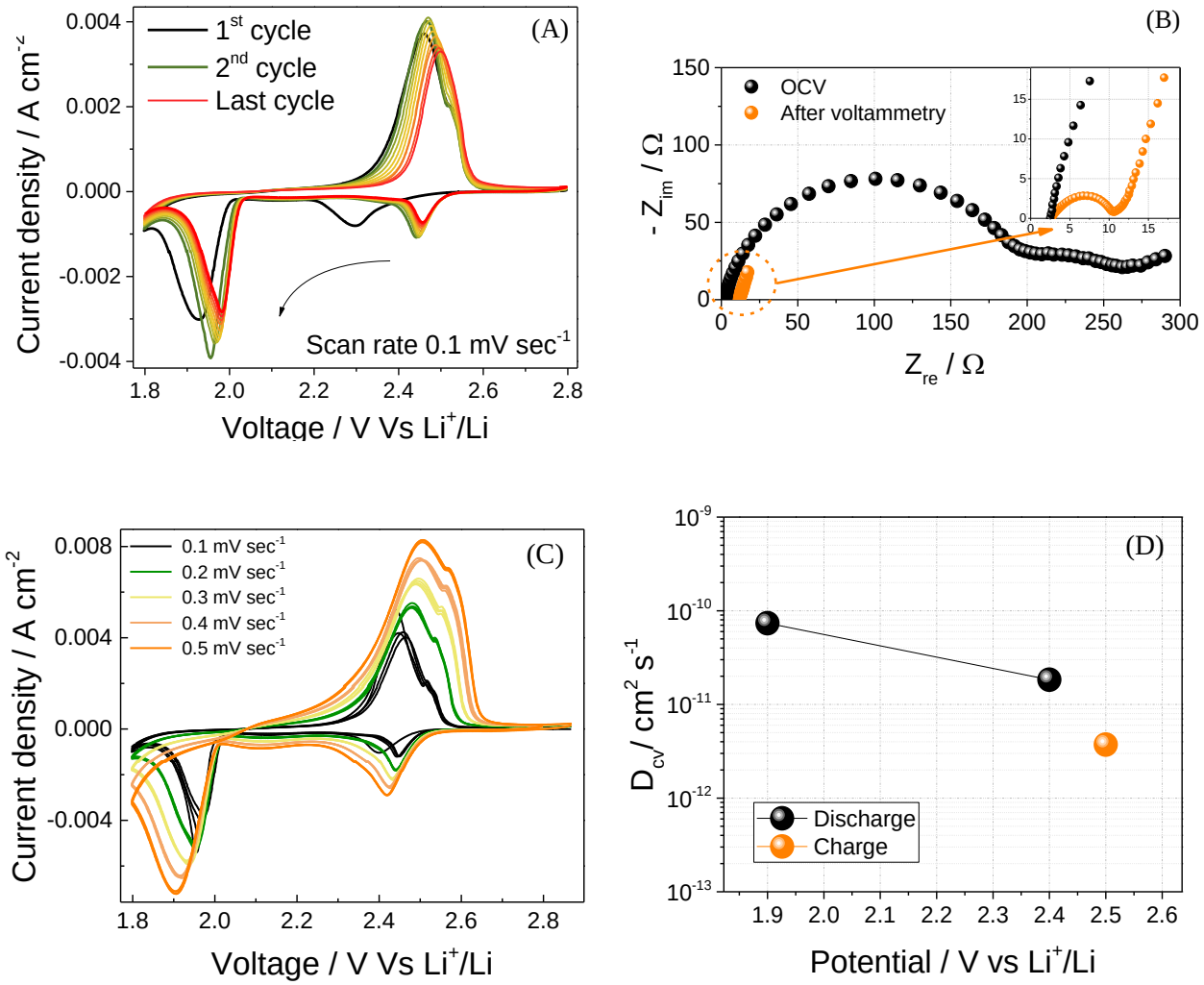

Figure 5. (A) Cyclic Voltammetry (CV) tests of the S-MWCNTs working electrode in tree-electrode using lithium metal as reference and counter electrode and the DEGDME-LiTFSI-$LiNO_3$ electrolyte performed in a potential range of 1.8 V - 2.9 V with a scan rate of 0.1 mV s^{-1}, and (B) impedance spectra of the cell before and after the CV test. (C) CV test performed in the same potential window by increasing the scan rate every three by 0.1 mV s-1 from 0.1 mV s^{-1} to 0.5 mV s^{-1}, and (D) Lithium ion diffusion coefficient calculated from the above CV tests by using the peak intensity (I_p), the scan rate (v) and the Randles-Sevcik equation (5). See experimental section for equation.

Figure 5D shows the expected increase of the Li^+-diffusion coefficient, hence of the electrode ion conductivity, by the ongoing of the lithiation, from about $3.7*10^{-12}$ cm^2 s^{-1} at the charged (de-lithiated) state at 2.5 V vs Li^+/Li, to about $1.7*10^{-11}$ cm^2 s^{-1} and $7.3*10^{-11}$ cm^2 s^{-1} at the discharged (lithiated) state at 2.4 V and 1.9 V vs Li^+/Li, respectively, which is in full agreement with the impedance decrease observed in Figure 5B.

An important parameter affecting the cell performance, particularly during galvanostatic cycling, is represented by the sulfur loading of the electrode [18]. Figure 6 reports the cycling trends of the Li/DEGDME-LiTFSI $LiNO_3$/S-MWCNTs cells with a sulfur content increasing from 2 to 4 mg cm^{-2} in the 1.9 V – 2.8 V range. The voltage profile of Figure 6A shows a capacity of about 1100 mAh g^{-1} (66% of the theoretical value) for the cell with sulfur loading of 2 mg cm^{-2} at C/3 rate, which increases at the same c-rate to about 1200 mAh g^{-1} (72% of the theoretical value) for the cells using electrodes with a sulfur loading of 2.5 and 3 mg cm^{-2}, most likely due to an optimal ratio between MWCNTs and S promoting efficient lithium ions conduction [60]. It is worth mentioning that the cell with sulfur loading of 4 mg cm^{-2} requires a lower C-rate (C/8 instead of C/3) for allowing suitable operation with a capacity of 1300 mAh g^{-1} (78% of the theoretical value), due to excessive polarization at the higher C-rates. Indeed, 1C current remarkably increases from 3.4 mA cm^{-2} for electrode loading of 2 mg cm^{-2} to about 7 mA cm^{-2} for electrode loading of 4 mg cm^{-2}, which may actually lead to cell polarization due to several factors, including insufficient electrode and electrolyte conductivity [61]. Despite the lower c-rate, the cycling tests in Figure 6B and inset evidence a remarkable increase of the areal capacity, i.e., the value normalized by the electrode geometric surface, from 2, 3 and 3.5 mAh cm^{-2} for the cell employing a sulfur loading of 2, 2.5 and 3 mg cm^{-2}, respectively, to 5.3 mAh cm^{-2} for the cell using a sulfur loading of 4 mg cm^{-2}, which represents a very suitable characteristic for the employment of the materials in scaled-up lithium-sulfur cell in line with the high performance LIBs.

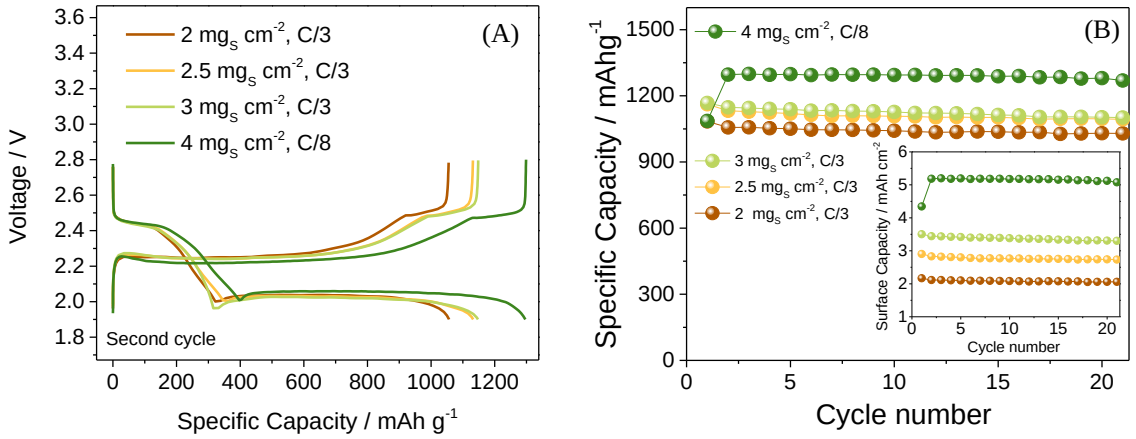

Figure 6. (A) Voltage profile and (B) cycling trends of a Li/S 2032-coin cells using the DEGDME-LiTFSI-$LiNO_3$ electrolyte and S-MWCNTs electrodes with increasing sulfur loading. The cycling rate is C/3 for the cells with sulfur loading of 2, 2.5 and 3 mg cm^{-2}, and C/8 for the cell with sulfur loading of 4 mg cm^{-2} (1C = 1675 mA g^{-1}). Voltage limits 1.9 V - 2.8 V. Temperature 23°C. The figure inset shows the corresponding surface capacity (mA cm^{-2}) calculated with respect to the geometric area of the electrodes.

The cycling ability of the Li/DEGDME-LiTFSI $LiNO_3$/S-MWCNTs cell is evaluated by galvanostatic cycling performed at various currents as well as at a constant c-rate, using an electrode with a sulfur loading of about 3 mg cm^{-2} (Figure 7). The cycling trend (Figure 7A) and voltage profiles (Figure 7B) of the rate capability test performed by increasing the current within 1.9 V and 2.8 V reveal a remarkable performance, with a delivered capacity ranging from 1200 mAh g^{-1} at C/10 to about 850 mAh g^{-1} at C/2 (1C = 1675 mAh g^{-1}), and limited charge/discharge polarization. At the higher c-rate (1C), the figure evidences a continuous increase of the capacity from 350 to about 500 mAh g^{-1}, and an initially high polarization subsequently decreasing by the 3 cycles of the test. This behavior may be justified by the cell resistance decrease and the Li^+-diffusion coefficient increase upon cycling, already observed in Figure 5 by EIS and CV, respectively. The cycling test performed at a constant rate of C/3 reported in Figure 7C, and the corresponding voltage profiles in Figure 7D, show an initial capacity of about 1100 mAh g^{-1}

delivered with an efficiency approaching 100% and very low polarization. The figure evidences a capacity decrease and a final stabilization at about 900 mAh g^{-1} over 120 cycles, as most likely due to slight electrode dissolution already observed by the CV test in Figure 5A. Interestingly, the cycling test at 1C reported in figure 7E reveals the electrode activation mentioned during the discussion of the rate capability test, with a capacity increasing by the initial 25 cycles from 350 mAh g^{-1} to the remarkable value 890 mAh g^{-1}, which remains very stable over the whole test. This trend is mainly ascribed to the increase of ionic and electronic conductivity of the electrode promoted by the reaction of the insulating sulfur with lithium [14,60], and to increased wetting of the electrode by time evolution [62,63], as indeed demonstrated by the relevant decrease of the electrode impedance during cyclic voltammetry observed in Figure 5B. The activation process and consequent impedance reduction leads to the decrease of the charge/discharge polarization, and to the increase of the cell capacity, particularly at high c-rate (1C) taking into account the restricted cell cutoff, i.e., 1.8-2.8 V. Figure 7E reveals a decrease of the cell efficiency from about 100% to 98%, and a subsequent rapid increase to 100% around the110^{th} cycle. This trend may be ascribed to a side polysulfide shuttle reaction due to partial SEI film dissolution at the lithium surface, and fast reconsolidation as also suggested by Figure 2 (A, B) reporting the electrochemical and chemical characteristics of the lithium/electrolyte interface [51]. A further proof of the reduction of the cell resistance by cycling is given by the voltage profiles of the same cell reported in Figure 7F, which show a notable decrease of the cell polarization from the first to the last cycle of the test which is in line with the EIS measurement observed in Figure 5B.

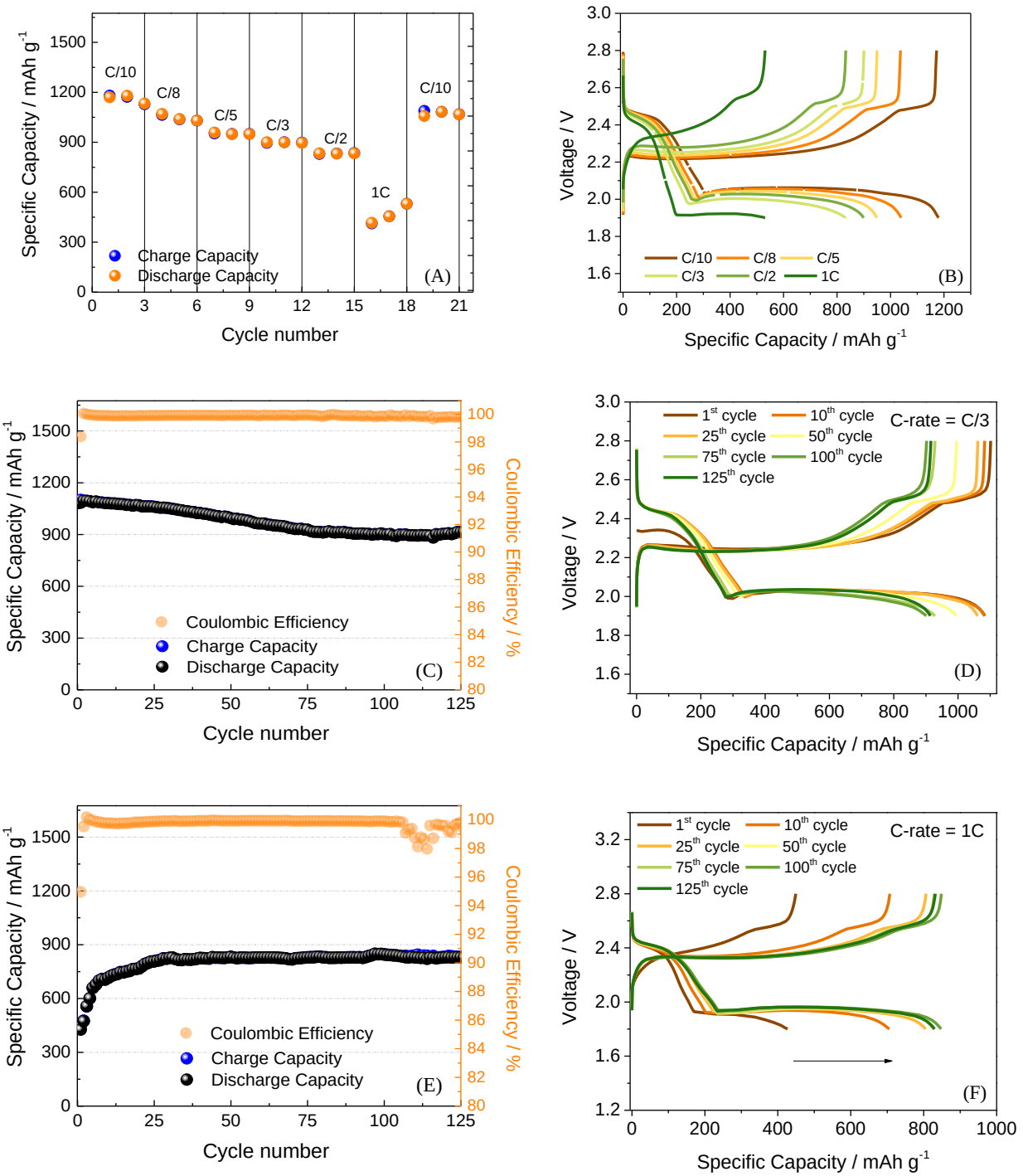

Figure 7. (A) Rate capability cycling behavior performed at C/10, C/8, C/5, C/3, C/2 and 1C (1C = 1675 mA g^{-1}), and (B) corresponding voltage profiles of a Li/S 2032-coin cell using the DEGDME-LiTFSI-$LiNO_3$ electrolyte and S-MWCNTs electrode. Prolonged cycling behavior and voltage profile of selected cycles of a Li/S 2032-coin cell using the DEGDME-LiTFSI-$LiNO_3$ electrolyte and S-MWCNTs electrode at a c-rate of C/3 (C, D) and 1C (E, F), respectively. Sulfur loading 3 mg cm^{-2}. Voltage limits 1.9 V – 2.8 V at C/3 and 1.8 V – 2.8 V at 1C. Temperature 23°C.

Conclusions

A DEGDME-LiTFSI electrolyte with added $LiNO_3$ is proposed as suitable solution for use in efficient and high performance Li/S cell, in combination with an electrode formed by combining sulfur and MWCNTs. The cell advantageously combines the low-flammability of the electrolyte, the low cost and the high performances of the electrode materials. The battery exploits suitable characteristics of the electrolyte such as high conductivity (of about of 10^{-2} S cm ^{1}), low ion association degree, an apparent lithium transport number of 0.5, as well as a relevant chemical and electrochemical stability. Furthermore, an optimized morphology of the electrode, consisting of spherical shape particles in which the MWCNTs shell coats the sulfur core, and the use of a suitable carbon cloth as the support, allow the cell to achieve a maximum capacity of 1300 mAh g^{-1} using a loading as high as 4 mg cm^{-2}, which is reflected into a practical areal capacity higher than 5 mAh cm^{-2}. Actually, the increase of the sulfur loading in the cathode represents one to the most relevant challenges of the Li/S cell. However, a too high sulfur loading, such as the one reported by the proof of concept batteries with S content ranging from 10 mg cm^{-2} to 30 mg cm^{-2} [60,61], may be reflected into a very low current rate, high polarization, poor coulombic efficiency, and low mass utilization. Instead, the sulfur content ranging between 2 and 4 mg cm^{-2} used in this work, and suggested by other papers [18,28], despite not the highest possible, represents a suitable compromise for achieving at the same time a high performances and a satisfactory practical capacity. Interestingly, the electrode material shows an increase of the lithium diffusion coefficient from $3.7*10^{-12}$ cm^2 s^{-1} to 7.3 10^{-11} cm^2 s ^{1} by lithiation process, as revealed by CV at various scan rates, which leads to a remarkable decrease of the cell resistance measured by EIS. This phenomenon is particularly relevant for cells cycling at the higher c-rates (1C) which undergo an activation process characterized an increase of the delivered capacity and a decrease of the polarization. Hence, the Li/S cell herein studied delivers a specific capacity exceeding 900 mAh g^{-1} and a with a coulombic efficiency approaching 100% for over 120 cycles and Considering a working voltage of 2 V and the above capacity, we may calculate for the battery a theoretical

energy density of 1800 Wh kg^{-1} which may be reflected into a practical energy over 400 Wh kg^{-1}, i.e., a value much higher than that of the 200 Wh kg^{-1} ascribed to the most diffused commercial lithium ion battery [64]. This characteristic, the relevant safety content of the electrolyte and the low expected cost of the employed materials suggest the cell as a high energy storage system for next generation applications, such as EVs. Certainly, the use of more economically sustainable carbons is a very attractive challenge for the development of a lithium-sulfur cell of practical application, which is therefore under consideration and study in our laboratories.

Acknowledgements

This work was supported by the grant "Fondo di Ateneo per la Ricerca Locale FAR 2016" and the collaboration project “Accordo di Collaborazione Quadro 2015” between University of Ferrara (Department of Chemical and Pharmaceutical Sciences) and Sapienza University of Rome (Department of Chemistry). The authors thank Daniela Palmeri (Electronic Microscopy Centre, Department of Chemical and Pharmaceutical Sciences) University of Ferrara, Italy) for performing electron microscopy images. The NMR measurements at Hunter College were supported by a grant from the U.S. Office of Naval Research, and the NMR Facility is supported in part by a National Institutes of Health RCMI infrastructure grant (MD007599)

References

[1] M.S. Whittingham, History, Evolution, and Future Status of Energy Storage, Proc. IEEE. 100 (2012) 1518–1534. doi:10.1109/JPROC.2012.2190170.

[2] B. Scrosati, History of lithium batteries, J. Solid State Electrochem. 15 (2011) 1623–1630. doi:10.1007/s10008-011-1386-8.

[3] C.D. Thomas, A. Cameron, R.E. Green, M. Bakkenes, L.J. Beaumont, Y.C. Collingham, et al., Extinction risk from climate change, Nature. 427 (2004) 145–148. doi:10.1038/nature02121.

[4] C. McGlade, P. Ekins, The geographical distribution of fossil fuels unused when limiting global warming to 2 °C, Nature. 517 (2015) 187–190. doi:10.1038/nature14016.

[5] O. Ellabban, H. Abu-Rub, F. Blaabjerg, Renewable energy resources: Current status, future prospects and their enabling technology, Renew. Sustain. Energy Rev. 39 (2014) 748–764. doi:10.1016/j.rser.2014.07.113.

[6] L. Croguennec, M.R. Palacin, Recent Achievements on Inorganic Electrode Materials for Lithium-Ion Batteries, J. Am. Chem. Soc. 137 (2015) 3140–3156. doi:10.1021/ja507828x.

[7] L. Ma, K.E. Hendrickson, S. Wei, L.A. Archer, Nanomaterials: Science and applications in the lithium–sulfur battery, Nano Today. 10 (2015) 315–338. doi:10.1016/j.nantod.2015.04.011.

[8] C. Barchasz, F. Molton, C. Duboc, Lithium/Sulfur Cell Discharge Mechanism: An Original Approach for Intermediate Species Identification, Anal. Chem. 84 (2012) 3973–3980. doi:10.1021/ac2032244.

[9] C. Sang-Eun, K. Ki-Seok, C. Ji-Hoon, K. Sun-Wook, C. Eog-Yong, K. Hee-Tak, 082 Rechargeable Lithium Sulfur Battery, J. Electrochem. Soc. 150 (2003) A796. doi:10.1149/1.1571532.

[10] S. Waluš, C. Barchasz, R. Bouchet, J.C. Leprêtre, J.F. Colin, J.F. Martin, et al., Lithium/Sulfur Batteries Upon Cycling: Structural Modifications and Species Quantification by in Situ and Operando X-Ray Diffraction Spectroscopy, Adv. Energy Mater. 5 (2015) 1500165. doi:10.1002/aenm.201500165.

[11] J. Xiao, J.Z. Hu, H. Chen, M. Vijayakumar, J. Zheng, H. Pan, et al., Following the Transient Reactions in Lithium–Sulfur Batteries Using an In Situ Nuclear Magnetic Resonance Technique, Nano Lett. 15 (2015) 3309–3316. doi:10.1021/acs.nanolett.5b00521.

[12] Y. Gorlin, M.U.M. Patel, A. Freiberg, Q. He, M. Piana, M. Tromp, et al., Understanding the

Charging Mechanism of Lithium-Sulfur Batteries Using Spatially Resolved Operando X-Ray Absorption Spectroscopy, J. Electrochem. Soc. 163 (2016) A930–A939. doi:10.1149/2.0631606jes.

[13] Q. Wang, J. Zheng, E. Walter, H. Pan, D. Lv, P. Zuo, et al., Direct Observation of Sulfur Radicals as Reaction Media in Lithium Sulfur Batteries, J. Electrochem. Soc. 162 (2015) A474–A478. doi:10.1149/2.0851503jes.

[14] M.R. Busche, P. Adelhelm, H. Sommer, H. Schneider, K. Leitner, J. Janek, Systematical electrochemical study on the parasitic shuttle-effect in lithium-sulfur-cells at different temperatures and different rates, J. Power Sources. 259 (2014) 289–299. doi:10.1016/j.jpowsour.2014.02.075.

[15] W. Wang, Y. Wang, Y. Huang, C. Huang, Z. Yu, H. Zhang, et al., The electrochemical performance of lithium-sulfur batteries with LiClO 4 DOL/DME electrolyte, J. Appl. Electrochem. 40 (2010) 321–325. doi:10.1007/s10800-009-9978-z.

[16] J. Kim, D.J. Lee, H.G. Jung, Y.K. Sun, J. Hassoun, B. Scrosati, An advanced lithium-sulfur battery, Adv. Funct. Mater. 23 (2013) 1076–1080. doi:10.1002/adfm.201200689.

[17] L. Carbone, M. Gobet, J. Peng, M. Devany, B. Scrosati, S. Greenbaum, et al., Comparative Study of Ether-Based Electrolytes for Application in Lithium-Sulfur Battery, ACS Appl. Mater. Interfaces. 7 (2015). doi:10.1021/acsami.5b02160.

[18] L. Qie, C. Zu, A. Manthiram, A High Energy Lithium-Sulfur Battery with Ultrahigh-Loading Lithium Polysulfide Cathode and its Failure Mechanism, Adv. Energy Mater. 6 (2016). doi:10.1002/aenm.201502459.

[19] A. Rosenman, R. Elazari, G. Salitra, E. Markevich, D. Aurbach, A. Garsuch, The Effect of Interactions and Reduction Products of LiNO3, the Anti-Shuttle Agent, in Li-S Battery Systems, J. Electrochem. Soc. 162 (2015) A470–A473. doi:10.1149/2.0861503jes.

[20] W. Li, H. Yao, K. Yan, G. Zheng, Z. Liang, Y.-M. Chiang, et al., The synergetic effect of lithium polysulfide and lithium nitrate to prevent lithium dendrite growth., Nat. Commun. 6 (2015) 7436. doi:10.1038/ncomms8436.

[21] S. Xiong, K. Xie, Y. Diao, X. Hong, Characterization of the solid electrolyte interphase on lithium anode for preventing the shuttle mechanism in lithium-sulfur batteries, J. Power Sources. 246 (2014) 840–845. doi:10.1016/j.jpowsour.2013.08.041.

[22] Y.S. Su, A. Manthiram, Lithium-sulphur batteries with a microporous carbon paper as a bifunctional interlayer, Nat Commun. 3 (2012) 1166. doi:10.1038/ncomms2163.

[23] J.Y. Hwang, H.M. Kim, S.K. Lee, J.H. Lee, A. Abouimrane, M.A. Khaleel, et al., High-Energy, High-Rate, Lithium-Sulfur Batteries: Synergetic Effect of Hollow TiO2-Webbed Carbon Nanotubes and a Dual Functional Carbon-Paper Interlayer, Adv. Energy Mater. 6 (2016) 1–7. doi:10.1002/aenm.201501480.

[24] M.S. Kim, L. Ma, S. Choudhury, S.S. Moganty, S. Wei, L.A. Archer, Fabricating multifunctional nanoparticle membranes by a fast layer-by-layer Langmuir–Blodgett process: application in lithium–sulfur batteries, J. Mater. Chem. A. 4 (2016) 14709–14719. doi:10.1039/C6TA06018H.

[25] Z. Yuan, H.-J. Peng, T.-Z. Hou, J.-Q. Huang, C.-M. Chen, D.-W. Wang, et al., Powering Lithium–Sulfur Battery Performance by Propelling Polysulfide Redox at Sulfiphilic Hosts, Nano Lett. 16 (2016) 519–527. doi:10.1021/acs.nanolett.5b04166.

[26] X. Liang, C.Y. Kwok, F. Lodi-Marzano, Q. Pang, M. Cuisinier, H. Huang, et al., Tuning Transition Metal Oxide-Sulfur Interactions for Long Life Lithium Sulfur Batteries: The "goldilocks" Principle, Adv. Energy Mater. 6 (2016) 1–9. doi:10.1002/aenm.201501636.

[27] X. Liang, C. Hart, Q. Pang, A. Garsuch, T. Weiss, L.F. Nazar, A highly efficient polysulfide mediator for lithium–sulfur batteries, Nat. Commun. 6 (2015) 5682.

doi:10.1038/ncomms6682.

[28] W. Li, Z. Liang, Z. Lu, H. Yao, Z.W. Seh, K. Yan, et al., A Sulfur Cathode with Pomegranate-Like Cluster Structure, Adv. Energy Mater. 5 (2015). doi:10.1002/aenm.201500211.

[29] B. Wang, Y. Wen, D. Ye, H. Yu, B. Sun, G. Wang, et al., Dual protection of sulfur by carbon nanospheres and graphene sheets for lithium-sulfur batteries, Chem. - A Eur. J. 20 (2014) 5224–5230. doi:10.1002/chem.201400385.

[30] Y. Yang, G. Yu, J.J. Cha, H. Wu, M. Vosgueritchian, Y. Yao, et al., Improving the performance of lithium-sulfur batteries by conductive polymer coating, ACS Nano. 5 (2011) 9187–9193. doi:10.1021/nn203436j.

[31] H. Sohn, M.L. Gordin, T. Xu, S. Chen, D. Lv, J. Song, et al., Porous spherical carbon/sulfur nanocomposites by aerosol-assisted synthesis: The effect of pore structure and morphology on their electrochemical performance as lithium/sulfur battery cathodes, ACS Appl. Mater. Interfaces. 6 (2014) 7596–7606.

[32] D. Sharon, D. Hirsberg, M. Afri, F. Chesneau, R. Lavi, A. a. Frimer, et al., Catalytic Behavior of Lithium Nitrate in Li-O 2 Cells, ACS Appl. Mater. Interfaces. 7 (2015) 16590–16600. doi:10.1021/acsami.5b04145.

[33] Y. Choquette, Sulfamides and Glymes as Aprotic Solvents for Lithium Batteries, J. Electrochem. Soc. 145 (1998) 3500. doi:10.1149/1.1838834.

[34] D. Aurbach, E. Granot, The study of electrolyte solutions based on solvents from the “glyme” family (linear polyethers) for secondary Li battery systems, Electrochim. Acta. 42 (1997) 697–718. doi:10.1016/S0013-4686(96)00231-9.

[35] S.S. Jeong, Y.T. Lim, Y.J. Choi, G.B. Cho, K.W. Kim, H.J. Ahn, et al., Electrochemical properties of lithium sulfur cells using PEO polymer electrolytes prepared under three

different mixing conditions, 174 (2007) 745–750. doi:10.1016/j.jpowsour.2007.06.108.

[36] S.K. Lee, S.M. Oh, E. Park, B. Scrosati, J. Hassoun, M.S. Park, et al., Highly cyclable lithium-sulfur batteries with a dual-type sulfur cathode and a lithiated Si/SiO<inf>x</inf> nanosphere anode, Nano Lett. 15 (2015) 2863–2868. doi:10.1021/nl504460s.

[37] E.O. Stejskal, J.E. Tanner, Spin Diffusion Measurements: Spin Echoes in the Presence of a Time- Dependent Field Gradient, J. Chem. Phys. 42 (1965) 288–292. doi:10.1063/1.1695690.

[38] B. Boukamp, A Nonlinear Least Squares Fit procedure for analysis of immittance data of electrochemical systems, Solid State Ionics. 20 (1986) 31–44. doi:10.1016/0167-2738(86)90031-7.

[39] B.A. Boukamp, A package for impedance/admittance data analysis, Solid State Ionics. 18–19 (1986) 136–140. doi:10.1016/0167-2738(86)90100-1.

[40] D. Di Lecce, R. Brescia, A. Scarpellini, M. Prato, J. Hassoun, A High Voltage Olivine Cathode for Application in Lithium-Ion Batteries, ChemSusChem. 9 (2016) 223–230. doi:10.1002/cssc.201501330.

[41] E.C.S. Transactions, T.E. Society, I. Hanzu, T. Djenizian, P. Knauth, Electrical and Proton Conduction Properties of Amorphous TiO 2 Nanotubes Fabricated by Electrochemical Anodization, ECS Trans. 35 (2011) 21–31. doi:10.1149/1.3570842.

[42] L. Carbone, D. Di Lecce, M. Gobet, S. Munoz, M. Devany, S. Greenbaum, et al., Relevant Features of a Triethylene Glycol Dimethyl Ether-Based Electrolyte for Application in Lithium Battery, (2017). doi:10.1021/acsami.7b03235.

[43] D. Di Lecce, L. Carbone, V. Gancitano, J. Hassoun, Rechargeable lithium battery using non-flammable electrolyte based on tetraethylene glycol dimethyl ether and olivine cathodes, J. Power Sources. 334 (2016) 146–153. doi:10.1016/j.jpowsour.2016.09.164.

[44] L. Carbone, M. Gobet, J. Peng, M. Devany, B. Scrosati, S. Greenbaum, et al., Polyethylene glycol dimethyl ether (PEGDME)-based electrolyte for lithium metal battery, J. Power Sources. 299 (2015) 460–464. doi:10.1016/j.jpowsour.2015.08.090.

[45] D. Aurbach, E. Pollak, R. Elazari, G. Salitra, C.S. Kelley, J. Affinito, On the Surface Chemical Aspects of Very High Energy Density, Rechargeable Li–Sulfur Batteries, J. Electrochem. Soc. 156 (2009) A694. doi:10.1149/1.3148721.

[46] S.S. Zhang, Role of LiNO3 in rechargeable lithium/sulfur battery, Electrochim. Acta. 70 (2012) 344–348. doi:10.1016/j.electacta.2012.03.081.

[47] L. Carbone, J. Peng, M. Agostini, M. Gobet, M. Devany, B. Scrosati, et al., Carbon Composites for a High-Energy Lithium-Sulfur Battey with a Glyme-Based Electrolyte, ChemElectroChem. (2016) 1–8. doi:10.1002/celc.201600586.

[48] X. Tao, J. Wang, C. Liu, H. Wang, H. Yao, G. Zheng, et al., Balancing surface adsorption and diffusion of lithium-polysulfides on nonconductive oxides for lithium-sulfur battery design, Nat. Commun. 7 (2016) 11203. doi:10.1038/ncomms11203.

[49] J. Peng, L. Carbone, M. Gobet, J. Hassoun, M. Devany, S. Greenbaum, Natural Abundance Oxygen-17 NMR Investigation of Lithium Ion Solvation in Glyme-based Electrolytes, Electrochim. Acta. 213 (2016) 606–612. doi:10.1016/j.electacta.2016.07.144.

[50] J. Park, J. Hassoun, H. Jung, H. Kim, C.S. Yoon, I. Oh, et al., Influence of Temperature on Lithium − Oxygen Battery Behavior, Nano Lett. 13 (2013) 2971–2975. doi:10.1021/nl401439b.

[51] S. Xiong, K. Xie, Y. Diao, X. Hong, Properties of surface film on lithium anode with LiNO 3 as lithium salt in electrolyte solution for lithium-sulfur batteries, Electrochim. Acta. 83 (2012) 78–86. doi:10.1016/j.electacta.2012.07.118.

[52] S.S. Zhang, Effect of Discharge Cutoff Voltage on Reversibility of Lithium/Sulfur Batteries

with LiNO3-Contained Electrolyte, J. Electrochem. Soc. 159 (2012) A920–A923. doi:10.1149/2.002207jes.

[53] L. Gireaud, S. Grugeon, S. Laruelle, B. Yrieix, J.M. Tarascon, Lithium metal stripping/plating mechanisms studies: A metallurgical approach, Electrochem. Commun. 8 (2006) 1639–1649. doi:10.1016/j.elecom.2006.07.037.

[54] S.S. Zhang, Liquid electrolyte lithium/sulfur battery: Fundamental chemistry, problems, and solutions, J. Power Sources. 231 (2013) 153–162. doi:10.1016/j.jpowsour.2012.12.102.

[55] H. Kim, J.T. Lee, A. Magasinski, K. Zhao, Y. Liu, G. Yushin, In Situ TEM Observation of Electrochemical Lithiation of Sulfur Confined within Inner Cylindrical Pores of Carbon Nanotubes, Adv. Energy Mater. 5 (2015) 1501306. doi:10.1002/aenm.201501306.

[56] Y. V. Mikhaylik, J.R. Akridge, Polysulfide Shuttle Study in the Li/S Battery System, J. Electrochem. Soc. 151 (2004) A1969. doi:10.1149/1.1806394.

[57] B. Scrosati, J. Garche, Lithium batteries: Status, prospects and future, J. Power Sources. 195 (2010) 2419–2430. doi:10.1016/j.jpowsour.2009.11.048.

[58] 2015_Jun Liu - NanoLetters_Following the Transient Reactions in Lithium−Sulfur Batteries Using an in Situ NMR.pdf, (n.d.).

[59] S. Waluś, C. Barchasz, R. Bouchet, J.-C. Leprêtre, J.-F. Colin, J.-F. Martin, et al., Lithium/Sulfur Batteries Upon Cycling: Structural Modifications and Species Quantification by In Situ and Operando X-Ray Diffraction Spectroscopy, Adv. Energy Mater. 5 (2015) 1500165. doi:10.1002/aenm.201500165.

[60] N. Ding, S.W. Chien, T.S.A. Hor, Z. Liu, Y. Zong, Key parameters in design of lithium sulfur batteries, J. Power Sources. 269 (2014) 111–116. doi:10.1016/j.jpowsour.2014.07.008.

[61] S.-H. Chung, C.-H. Chang, A. Manthiram, A core–shell electrode for dynamically and

statically stable Li–S battery chemistry, Energy Environ. Sci. 9 (2016) 3188–3200. doi:10.1039/C6EE01280A.

[62] L. Xiao, Y. Cao, J. Xiao, B. Schwenzer, M.H. Engelhard, L. V. Saraf, et al., A soft approach to encapsulate sulfur: Polyaniline nanotubes for lithium-sulfur batteries with long cycle life, Adv. Mater. 24 (2012) 1176–1181. doi:10.1002/adma.201103392.

[63] S. Urbonaite, T. Poux, P. Novák, Progress Towards Commercially Viable Li-S Battery Cells, Adv. Energy Mater. (2015) n/a-n/a. doi:10.1002/aenm.201500118.

[64] E.M. Erickson, C. Ghanty, D. Aurbach, New horizons for conventional lithium ion battery technology, J. Phys. Chem. Lett. 5 (2014) 3313–3324. doi:10.1021/jz501387m.

Graphical Abstract